Incremental Equations
for Soft Fibrous Materials

Michel Destrade

School of Mathematics, Statistics and Applied Mathematics
National University of Ireland Galway, Ireland.[*]

E-mail: `michel.destrade@nuigalway.ie`

Abstract. The general theory of nonlinear anisotropic elasticity is extended to describe small-amplitude motions and static deformations that can be superimposed on large pre-strains of fibre-reinforced solids. The linearised governing equations of incremental motion are derived. Then they are solved for some illustrative situations which reveal a wide spectrum of possible behaviours compared to the case of initially isotropic materials. Particular attention is paid to the propagation of homogeneous waves and to the formation of static wrinkles. These objects prove useful in the investigation of the issues of material (in the bulk) and geometrical (at boundaries) stability. Attempts are also made at modelling some experimental observations made on (isotropic) silicone and (anisotropic) biological soft tissues.
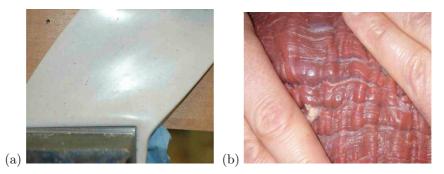
1 Introduction

Consider two rectangular solid blocks, one made of silicone, the other made of mammalian skeletal muscle ('meat'), and subject them to a large shear. The first block deforms smoothly and its surface remains flat; see Figure 1(a). The second block, however, experiences a form of buckling early on, as small-amplitude wrinkles appear on its surface. From visual inspection and intuition, we can come up with an explanation for these strikingly different behaviours. If we were careful in our moulding of the silicone block, we can safely assume that it is isotropic. On the other hand, the piece of meat is clearly anisotropic, as it is 'reinforced' with visible aligned fibres. When sheared, these fibres and/or their entanglements resist compression

---

and crumple early, lifting the surrounding tissue into a wavy pattern, with wavefronts at right-angles to the fibres; see Figure 1(b). Hence, although both blocks are soft and easily deformed, it is likely that they behave differently due to the absence or presence of fibres.
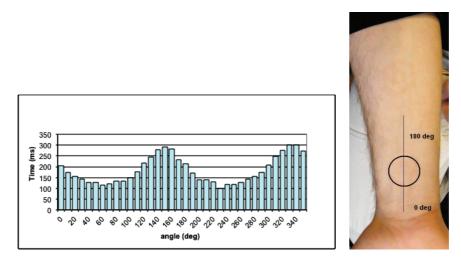

(a)
(b)

Figure 1. (a) A block of silicone subject to a large shear by hand; its surface remains flat and smooth. (b) A piece of meat sheared by hand, in a direction approximatively at 45° with respect to the fibres; its surface buckles early, with wrinkles forming at right-angle to the fibres.

From a mechanics point of view, we may now ask ourselves whether there exists a way of describing and predicting how the two blocks should behave in shear. As seen in the course of this chapter, it turns out that the simplest models of isotropic (for the silicone) and anisotropic (for the meat) *nonlinear incompressible elasticity* can indeed capture these effects. Of course the analysis itself is not easy and requires a good grasp of theoretical issues, physically-based modelling, and numerical analysis.

In order to model the small-amplitude wrinkles, we need to derive the *incremental equations of motion* of anisotropic non-linear elasticity. This procedure is described in Section 2; simply put, it relies on linearising the equations of motion in the neighbourhood of a static state of equilibrium corresponding to a large homogeneous deformation. These equations can be established in all generality, and in Section 3 we use them to study the *propagation of bulk waves* in deformed soft solids.

Indeed, wave propagation is a straightforward tool for figuring out if a solid is isotropic or not. Consider, for example, the experimental results displayed in Figure 2: they clearly show two privileged directions, along which a mechanical signal travels at different speeds than in other directions. Again, this can be captured by very simple models of nonlinear anisotropic elasticity. Deriving the speed v of a travelling wave explicitly also has an

Figure 2. The Reviscometer® records the information sent by a measurement probe (placed on the skin) which can be rotated to give the variation of acoustic perturbation speed with angle. The device measures the time it takes for an impulse generated by one needle sensor to reach another sensor 2mm away by travelling on the surface of the skin. Here, measurements were made every 10° on the forearm of a young female, and averaged over 6 experiments.

advantage from the point of view of constitutive modelling, as writing down the conditions for v^2 to be positive puts physically-based restrictions on the material parameters.

Finally in Section 4, armed with all the tools and knowledge required, we can at last tackle the problem raised by our observation of Figure 1. In that section we write down the *incremental equations of static equilibrium* (i.e. we take $v = 0$) for a perturbation which is sinusoidal on the surface of a sheared half-space (to describe the wavy pattern) and decays exponentially with depth inside the substrate (to describe near-surface wrinkles). Then we set out to solve these equations. For the isotropic model of choice (the neo-Hookean model), great analytical progress and results can be found, and they square well with experimental data. For the anisotropic models, we must turn to numerics. Thankfully, a host of tools is at our disposal to help us generate a robust method of resolution, based on the Stroh formalism and its extension to include the surface impedance method.

3

2   Incremental Equations

In this section we derive the equations governing the propagation of small-amplitude ('incremental') motions in anisotropic hyperelastic solids subjected to large static homogeneous deformations. The method of derivation is now well established and we omit certain details which can be found elsewhere; see references at the end of the chapter, in particular the CISM chapter by Ogden (2001). For simplicity we write the components of vectors and tensors in rectangular Cartesian coordinate systems, but the analysis can generalised to other systems of coordinates at little cost.

2.1   Large Static Pre-deformation

We consider that our solid is initially at rest in the *reference configuration* $\mathcal{B}_0$ (say). It is then brought to an equilibrium configuration (the *current configuration $\mathcal{B}$*, say) by the application of a pre-stress with measure $\boldsymbol{\sigma}$ (a Cauchy stress). Hence a point initially at $\boldsymbol{X}$ in $\mathcal{B}_0$ is at $\boldsymbol{x} = \boldsymbol{\chi}(\boldsymbol{X})$ in $\mathcal{B}$, where $\boldsymbol{\chi}$ is a one-to-one mapping; see Figure 3.
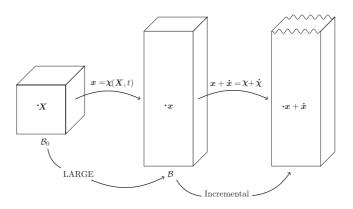

Figure 3. Sketch of the successive deformations taking place in the soft solid: first a large static homogeneous deformation, followed by an incremental motion.

The deformation $\boldsymbol{x} = \boldsymbol{\chi}\left(\boldsymbol{X}\right)$ is described by *deformation gradient* $\boldsymbol{F}$:

$$\boldsymbol{F} = \frac{\partial \boldsymbol{\chi}}{\partial \boldsymbol{X}}, \qquad F_{i\alpha} = \frac{\partial \chi_i}{\partial X_\alpha}. \tag{1}$$

Here the components of $\boldsymbol{F}$ are given in the $\boldsymbol{e}_i \otimes \boldsymbol{E}_j$ system, where $\boldsymbol{E}_i$ and $\boldsymbol{e}_i$ $(i = 1, 2, 3)$ form orthonormal vector bases in $\mathcal{B}_0$ and $\mathcal{B}$, respectively.

Let $J = \det \boldsymbol{F}$; this quantity measures the local volume changes, because it relates an elementary volume dV in $\mathcal{B}_0$ to its counterpart in $\mathcal{B}$ through

$$dv = JdV. \tag{2}$$

Using this identity, we may write the *conservation of mass* as follows

$$\int_{\mathcal{B}_0} \rho_0 dv = \int_{\mathcal{B}} \rho dv = \int_{\mathcal{B}_0} \rho JdV, \qquad \text{so that} \ \ \rho_0 = \rho J, \tag{3}$$

where ρ_0 and ρ are the mass densities per unit volume in $\mathcal{B}_0$ and $\mathcal{B}$, respectively.

Finally, we may write the *equations of equilibrium*, in the absence of body forces, as

$$\text{Div} \ \boldsymbol{S} = \boldsymbol{0}, \qquad \frac{\partial S_{\alpha i}}{\partial X_\alpha} = 0, \tag{4}$$

where $\boldsymbol{S} = J^{-1}\boldsymbol{F}\boldsymbol{\sigma}$ is the *nominal stress tensor*. We assume that the solid is hyperelastic, so that it possesses a *strain-energy density* $W = W(\boldsymbol{F})$ per unit mass. Then $\boldsymbol{S}$ is given by (Ogden, 2001),

$$\boldsymbol{S} = \frac{\partial W}{\partial \boldsymbol{F}}, \qquad S_{\alpha i} = \frac{\partial W}{\partial F_{i\alpha}}. \tag{5}$$

Notice here the convention used throughout the chapter for the ordering of the indices when differentiating tensors. For *incompressible* solids, volume changes are not permitted, so that $J = 1$ at all times. In that case $\boldsymbol{S}$ is given by

$$\boldsymbol{S} = \frac{\partial W}{\partial \boldsymbol{F}} - p\boldsymbol{F}^{-1}, \tag{6}$$

where p is a Lagrange multiplier, to be determined from boundary and/or initial conditions.

Finally, the *boundary conditions* are

$$\boldsymbol{S}^T \boldsymbol{N} = \boldsymbol{f} \ \text{on} \ \partial \mathcal{B}_0, \tag{7}$$

where $\boldsymbol{f}$ are the applied tractions and the upper script T denotes the transpose.

2.2 Increments

Now we 'increment' the quantities and equations encountered so far. In other words, we linearise them, using a right-arrow to mean 'is incremented

to', and a dot to denote an incremental quantity. Hence, for the increment of the deformation we have

$$\boldsymbol{x} = \boldsymbol{\chi}\left(\boldsymbol{X}\right) \quad \longrightarrow \quad \boldsymbol{x} + \dot{\boldsymbol{x}} = \boldsymbol{\chi}\left(\boldsymbol{X}\right) + \dot{\boldsymbol{\chi}}\left(\boldsymbol{X}, t\right). \tag{8}$$

But $\boldsymbol{X}$ can be seen as a function of $\boldsymbol{x}$ by writing $\boldsymbol{X} = \boldsymbol{\chi}^{-1}\left(\boldsymbol{x}\right)$, so that $\dot{\boldsymbol{\chi}}$ can also be seen as a function of $\boldsymbol{x}$. Then $\boldsymbol{u}\left(\boldsymbol{x}, t\right) \equiv \dot{\boldsymbol{\chi}}\left(\boldsymbol{x}, t\right)$ is called the *mechanical displacement.*

Next, we increment the deformation gradient:

$$\boldsymbol{F} = \frac{\partial \boldsymbol{\chi}}{\partial \boldsymbol{X}} \quad \longrightarrow \quad \boldsymbol{F} + \dot{\boldsymbol{F}}. \tag{9}$$

Here, using the chain rule, we find that

$$\dot{F}_{i\alpha} = \frac{\partial \dot{\chi}_i}{\partial X_\alpha} = \frac{\partial x_j}{\partial X_\alpha} \frac{\partial u_i}{\partial x_j} = F_{j\alpha} u_{i,j}, \qquad \text{or} \qquad \dot{\boldsymbol{F}} = \boldsymbol{\Gamma}\,\boldsymbol{F}, \tag{10}$$

where $\boldsymbol{\Gamma} = \text{grad } \boldsymbol{u}$ is the Eulerian *displacement gradient.*

Moving on to the increment of the nominal stress tensor, we have

$$\boldsymbol{S} = \boldsymbol{S}\left(\boldsymbol{F}\right) \rightarrow \boldsymbol{S} = \boldsymbol{S} + \dot{\boldsymbol{S}}, \quad \text{or} \quad S_{\alpha i}\left(F_{l\beta} + \dot{F}_{l\beta}\right) = S_{\alpha i}\left(F_{l\beta}\right) + \dot{S}_{\alpha i}\left(F_{l\beta}\right). \tag{11}$$

Here, using the chain rule and (10), we find that

$$\dot{S}_{\alpha i} = \frac{\partial S_{\alpha i}}{\partial F_{l\beta}} \dot{F}_{l\beta} = \frac{\partial S_{\alpha i}}{\partial F_{l\beta}} \Gamma_{lk} F_{k\beta}, \qquad \text{or} \qquad \dot{S}_{\alpha i} = \mathcal{A}_{\alpha i\beta l} \Gamma_{lk} F_{k\beta}, \tag{12}$$

where $\mathcal{A}_{\alpha i\beta l} = \partial S_{\alpha i}/\partial F_{l\beta}$ are the *fixed-reference moduli.* By (5), they are defined as

$$\mathcal{A}_{\alpha i\beta l} = \frac{\partial^2 W}{\partial F_{i\alpha}\partial F_{l\beta}}. \tag{13}$$

We can then increment the equations of equilibrium (4), as

$$\text{Div}\,\boldsymbol{S} = \boldsymbol{0} \quad \longrightarrow \quad \text{Div}\,\dot{\boldsymbol{S}} = \boldsymbol{0}, \qquad \text{or} \qquad \frac{\partial S_{\alpha i}}{\partial X_\alpha} \quad \longrightarrow \quad \frac{\partial \dot{S}_{\alpha i}}{\partial X_\alpha} = 0. \tag{14}$$

Integrating over the volume of the solid, we perform the following series of

operations,

$$\int_{\mathcal{B}_0} \text{Div}\,\dot{\boldsymbol{S}}\,dV = \int_{\partial\mathcal{B}_0} \dot{\boldsymbol{S}}^T \boldsymbol{N}\ dA \qquad \text{(divergence theorem)} \qquad (15)$$

$$= \int_{\partial\mathcal{B}} J^{-1}\dot{\boldsymbol{S}}^T \boldsymbol{F}^T \boldsymbol{n}\ da \qquad \text{(Nanson's formula)} \qquad (16)$$

$$= \int_{\partial\mathcal{B}} \left(J^{-1}\boldsymbol{F}\,\dot{\boldsymbol{S}}\right)^T \boldsymbol{n}\ da \qquad \text{(transpose of product)} \qquad (17)$$

$$= \int_{\mathcal{B}} \text{div}\left(J^{-1}\boldsymbol{F}\,\dot{\boldsymbol{S}}\right)\ dv \qquad \text{(divergence theorem)} \qquad (18)$$

so that the incremental equations of equilibrium can be put in the following equivalent (Eulerian) form:

$$\text{div}\,\boldsymbol{\Sigma} = \boldsymbol{0}, \qquad \frac{\partial \Sigma_{ji}}{\partial x_j} = 0. \qquad (19)$$

Here, the tensor $\boldsymbol{\Sigma}$ is defined as $\boldsymbol{\Sigma} = J^{-1}\boldsymbol{F}\,\dot{\boldsymbol{S}}$, with components

$$\Sigma_{ji} = J^{-1}F_{j\alpha}\dot{S}_{\alpha i} = J^{-1}F_{j\alpha}\mathcal{A}_{\alpha i\beta l}\Gamma_{lk}F_{k\beta}, \qquad \text{or} \qquad \Sigma_{ji} = \mathcal{A}_{0jikl}\Gamma_{lk}, \qquad (20)$$

where the *instantaneous elastic moduli* are the following components of the fourth-order tensor $\boldsymbol{\mathcal{A}}_0$,

$$\mathcal{A}_{0jikl} = J^{-1}\mathcal{A}_{\alpha i\beta l}F_{j\alpha}F_{k\beta} = J^{-1}\frac{\partial^2 W}{\partial F_{i\alpha}\partial F_{l\beta}}F_{j\alpha}F_{k\beta}. \qquad (21)$$

Let us increment the boundary conditions (7) where the applied tractions $\boldsymbol{f}$ are considered to correspond to a dead-load (i.e. $\boldsymbol{f}$ is constant).

$$\boldsymbol{S}^T \boldsymbol{N} = \boldsymbol{f} \quad \longrightarrow \quad \dot{\boldsymbol{S}}^T \boldsymbol{N} = \dot{\boldsymbol{f}} = \boldsymbol{0} \quad \text{on } \partial\mathcal{B}_0. \qquad (22)$$

Using Nanson's formula, we have the equivalent Eulerian form:

$$\boldsymbol{\Sigma}^T \boldsymbol{n} = \boldsymbol{0} \quad \text{on } \partial\mathcal{B}. \qquad (23)$$

In the case where the solid is incompressible, we need to increment the constraint of incompressibility $\det \boldsymbol{F} = 1$. Recalling that $\dfrac{\text{d}}{\text{d}\tau}(\det \boldsymbol{A}) = (\det \boldsymbol{A})\,\text{tr}\left(\dfrac{d\boldsymbol{A}}{d\tau}\boldsymbol{A}^{-1}\right)$, we find

$$J = 1 \quad \longrightarrow \quad J\,\text{tr}\left(\dot{\boldsymbol{F}}\boldsymbol{F}^{-1}\right) = 0, \qquad \text{i.e.} \qquad \text{tr}\,\boldsymbol{\Gamma} = u_{i,i} = 0. \qquad (24)$$

Then the increment of the nominal stress for incompressible solids (6) is found by incrementing the following identity,

$$\boldsymbol{F}\,\boldsymbol{F}^{-1} = \boldsymbol{I} \quad \longrightarrow \quad \dot{\boldsymbol{F}}\,\boldsymbol{F}^{-1} + \boldsymbol{F}(\overline{\dot{\boldsymbol{F}^{-1}}}) = \boldsymbol{0}, \tag{25}$$

so that

$$\boldsymbol{S} \quad \longrightarrow \quad \dot{\boldsymbol{S}} = \boldsymbol{\mathcal{A}}\,\boldsymbol{F}\boldsymbol{\Gamma} - \dot{p}\boldsymbol{F}^{-1} + p\boldsymbol{F}^{-1}\,\boldsymbol{\Gamma}, \tag{26}$$

and $\boldsymbol{\Sigma} = J^{-1}\boldsymbol{F}\,\dot{\boldsymbol{S}} = \boldsymbol{F}\,\dot{\boldsymbol{S}}$ is now given by

$$\boldsymbol{\Sigma} = \boldsymbol{\mathcal{A}}_0\,\boldsymbol{\Gamma} - \dot{p}\boldsymbol{I} + p\boldsymbol{\Gamma}, \qquad \Sigma_{ji} = \mathcal{A}_{0jikl}u_{l,k} + \dot{p}\delta_{ji} + pu_{j,i}. \tag{27}$$

2.3 Elastic Moduli

Here we focus on the instantaneous elastic moduli, which are given by (21), with $J = 1$ for incompressible materials. By swapping ji with kl in (21), and taking into account that α and β are dummy indices, we obtain

$$\mathcal{A}_{0klji} = \mathcal{A}_{0jikl}, \tag{28}$$

the so-called *major symmetries*. Owing to those symmetries, we can count that in general, there are at most 45 independent instantaneous moduli.

The moduli do not possess the 'minor' symmetries, and $\mathcal{A}_{0jikl} \neq \mathcal{A}_{0ijkl}$ in general. We may find out what the difference $\mathcal{A}_{0jikl} - \mathcal{A}_{0ijkl}$ is. First, recall that the Cauchy stress $\boldsymbol{\sigma}$ is symmetric: $\boldsymbol{\sigma} = J^{-1}\boldsymbol{F}\,\boldsymbol{S} = \boldsymbol{\sigma}^T$. Hence, by incrementing,

$$\boldsymbol{F}\,\boldsymbol{S} = (\boldsymbol{F}\,\boldsymbol{S})^T \quad \longrightarrow \quad \dot{\boldsymbol{F}}\,\boldsymbol{S} + \boldsymbol{F}\,\dot{\boldsymbol{S}} = (\dot{\boldsymbol{F}}\,\boldsymbol{S} + \boldsymbol{F}\,\dot{\boldsymbol{S}})^T, \tag{29}$$

we get, using (10), (12) and (21),

$$\begin{aligned}
&\boldsymbol{\Gamma}\boldsymbol{F}\boldsymbol{S} + J\boldsymbol{\mathcal{A}_0}\boldsymbol{\Gamma} = (\boldsymbol{\Gamma}\boldsymbol{F}\boldsymbol{S} + J\boldsymbol{\mathcal{A}_0}\boldsymbol{\Gamma})^T, \\
&\boldsymbol{\Gamma}\boldsymbol{\sigma} + \boldsymbol{\mathcal{A}_0}\boldsymbol{\Gamma} = (\boldsymbol{\Gamma}\boldsymbol{\sigma} + \boldsymbol{\mathcal{A}_0}\boldsymbol{\Gamma})^T, \\
&\Gamma_{jk}\sigma_{ki} + \mathcal{A}_{0jikl}\Gamma_{lk} = \Gamma_{ik}\sigma_{kj} + \mathcal{A}_{0ijkl}\Gamma_{lk}, \\
&\sigma_{ki}\delta_{jl}\Gamma_{lk} + \mathcal{A}_{0jikl}\Gamma_{lk} = \sigma_{kj}\delta_{il}\Gamma_{lk} + \mathcal{A}_{0ijkl}\Gamma_{lk}.
\end{aligned} \tag{30}$$

Collecting the terms in Γ_{lk}, we reach the conclusion that (Chadwick, 1997)

$$\mathcal{A}_{0jikl} - \mathcal{A}_{0ijkl} = \sigma_{jk}\delta_{il} - \sigma_{ik}\delta_{jl}. \tag{31}$$

In particular, $\mathcal{A}_{0ijji} - \mathcal{A}_{0jiij} = \mathcal{A}_{0ijij} - \sigma_{ii}$ when $i \neq j$ (no sum).

For incompressible solids, the derivation of the difference in the moduli is similar, based on (26). We then find that (Chadwick, 1997)

$$\mathcal{A}_{0jikl} - \mathcal{A}_{0ijkl} = (\sigma_{jk} + p\delta_{jk})\,\delta_{il} - (\sigma_{ik} + p\delta_{ik})\,\delta_{jl}. \tag{32}$$

In particular, we have

$$\mathcal{A}_{0jiij} - \mathcal{A}_{0ijij} = -\sigma_{ii} - p. \tag{33}$$

As explained elsewhere in this book, for general nonlinear materials with two families of fibres, one oriented along $\boldsymbol{M}$, the other along $\boldsymbol{M'}$ (in $\mathcal{B}_0$), the strain energy density W can always be written as a function of the following eight invariants

$$\begin{cases} I_1 = \text{tr}\,(\boldsymbol{C}), \\ I_2 = \frac{1}{2}\left[(\text{tr}\boldsymbol{C})^2 - \text{tr}\,(\boldsymbol{C}^2)\right] = I_3\,\text{tr}\,(\boldsymbol{C}^{-1}), \\ I_3 = \det\,(\boldsymbol{C}), \\ I_4 = \boldsymbol{M} \cdot \boldsymbol{C}\boldsymbol{M} = \boldsymbol{m} \cdot \boldsymbol{m}, \\ I_5 = \boldsymbol{M} \cdot \boldsymbol{C}^2\boldsymbol{M} = \boldsymbol{m} \cdot \boldsymbol{B}\boldsymbol{m}, \\ I_6 = \boldsymbol{M'} \cdot \boldsymbol{C}\boldsymbol{M'} = \boldsymbol{m'} \cdot \boldsymbol{m'}, \\ I_7 = \boldsymbol{M'} \cdot \boldsymbol{C}^2\boldsymbol{M'} = \boldsymbol{m} \cdot \boldsymbol{B}\boldsymbol{m'}, \\ I_8 = \boldsymbol{M} \cdot \boldsymbol{C}\boldsymbol{M'} = \boldsymbol{m} \cdot \boldsymbol{m'}, \end{cases} \tag{34}$$

where $\boldsymbol{B} = \boldsymbol{F}\boldsymbol{F}^T$ is the left Cauchy–Green deformation tensor, $\boldsymbol{m} = \boldsymbol{F}\boldsymbol{M}$, $\boldsymbol{m'} = \boldsymbol{F}\boldsymbol{M'}$, and $\boldsymbol{C} = \boldsymbol{F}^T\boldsymbol{F}$ is the right Cauchy–Green deformation tensor. Hence $W = W(I_1, I_2, \ldots, I_8)$ and we can then use the chain rule to compute the moduli given by (21). For this task, we need expressions for the first derivatives of the eight invariants with respect to $\boldsymbol{F}$. They are (Ogden, 2007)

$$\frac{\partial I_1}{\partial F_{i\alpha}} = 2F_{i\alpha}, \qquad \frac{\partial I_2}{\partial F_{i\alpha}} = 2(C_{\gamma\gamma}F_{i\alpha} - C_{\alpha\gamma}F_{i\gamma}), \qquad \frac{\partial I_3}{\partial F_{i\alpha}} = 2I_3 F_{\alpha i}^{-1},$$

$$\frac{\partial I_4}{\partial F_{i\alpha}} = 2M_\alpha F_{i\gamma}M_\gamma, \qquad \frac{\partial I_5}{\partial F_{i\alpha}} = 2(F_{i\gamma}M_\gamma C_{\alpha\gamma}M_\beta + F_{i\gamma}C_{\gamma\beta}M_\beta M_\alpha),$$

$$\frac{\partial I_8}{\partial F_{i\alpha}} = F_{i\gamma}(M'_\alpha M_\gamma + M_\alpha M'_\gamma), \tag{35}$$

and the derivatives of I_6 and I_7 are found from those of I_4 and I_5 by replacing $\boldsymbol{M}$ with $\boldsymbol{M'}$. We also need expressions for the second derivatives. They read

$$\frac{\partial^2 I_1}{\partial F_{i\alpha}\partial F_{l\beta}} = 2\delta_{il}\delta_{\alpha\beta},$$

$$\frac{\partial^2 I_2}{\partial F_{i\alpha}\partial F_{l\beta}} = 2\left(2F_{i\alpha}F_{l\beta} - F_{i\beta}F_{l\alpha} + C_{\gamma\gamma}\delta_{il}\delta_{\alpha\beta} - B_{il}\delta_{\alpha\beta} - C_{\alpha\beta}\delta_{il}\right),$$

$$\frac{\partial^2 I_3}{\partial F_{i\alpha}\partial F_{l\beta}} = 2I_3\left(2F_{\alpha i}^{-1}F_{\beta l}^{-1} - F_{\alpha l}^{-1}F_{\beta i}^{-1}\right),$$

$$\frac{\partial^2 I_4}{\partial F_{i\alpha}\partial F_{l\beta}} = 2\delta_{il}M_\alpha M_\beta,$$

$$\frac{\partial^2 I_5}{\partial F_{i\alpha}\partial F_{l\beta}} = 2\left[\delta_{il}(C_{\alpha\gamma}M_\gamma M_\beta + C_{\beta\gamma}M_\gamma M_\alpha) + \delta_{\alpha\beta}F_{i\gamma}M_\gamma F_{l\delta}M_\delta\right.$$
$$\left. + F_{i\gamma}M_\gamma F_{l\alpha}M_\beta + F_{l\gamma}M_\gamma F_{i\beta}M_\alpha + B_{il}M_\alpha M_\beta\right].$$

$$(36)$$

Again, the expressions for the derivatives of I_6 and I_7 are found from those of I_4 and I_5 by replacing $\boldsymbol{M}$ with $\boldsymbol{M}'$. Finally,

$$\frac{\partial^2 I_8}{\partial F_{i\alpha}F_{l\beta}} = \delta_{il}(M'_\alpha M_\beta + M_\alpha M'_\beta). \tag{37}$$

Computing the instantaneous moduli from (21) and (35)–(37) is not that difficult in practice, and the process can be automated with a computer algebra system if needs be. Take the case of *incompressible solids reinforced with one family of parallel fibres*. Their strain-energy density is of the form

$$W = W(I_1, I_2, I_4, I_5), \tag{38}$$

only, because $I_3 = 1$ at all times. Then we find that

$$\begin{aligned}
\mathcal{A}_{0jikl} = {} & 2W_1\delta_{il}B_{jk} \\
& + 2W_2\left[2B_{ij}B_{kl} - B_{ik}B_{jl} - B_{il}B_{jk} + I_1\delta_{il}B_{jk} - \delta_{il}(\boldsymbol{B}^2)_{jk}\right] \\
& + 2W_4\delta_{il}m_j m_k \\
& + 2W_5\left[\delta_{il}(\boldsymbol{B}\boldsymbol{m})_j m_k + \delta_{il}(\boldsymbol{B}\boldsymbol{m})_k m_j\right. \\
& \qquad\qquad \left. + B_{jk}m_i m_l + B_{jl}m_i m_k + B_{ik}m_j m_l + B_{il}m_j m_k\right] \\
& + 4W_{11}B_{ij}B_{kl} \\
& + 4W_{22}(I_1\boldsymbol{B} - \boldsymbol{B}^2)_{ij}(I_1\boldsymbol{B} - \boldsymbol{B}^2)_{kl} \\
& + 4W_{12}\left[B_{ij}(I_1\boldsymbol{B} - \boldsymbol{B}^2)_{kl} + B_{kl}(I_1\boldsymbol{B} - \boldsymbol{B}^2)_{ij}\right] \\
& + 4W_{14}\left(B_{ij}m_k m_l + B_{kl}m_i m_j\right) \\
& + 4W_{24}\left[(I_1\boldsymbol{B} - \boldsymbol{B}^2)_{kl}m_i m_j + (I_1\boldsymbol{B} - \boldsymbol{B}^2)_{ij}m_k m_l\right] \\
& + 4W_{44}m_i m_j m_k m_l
\end{aligned}$$

$$+ 4W_{55} \left[(\boldsymbol{Bm})_i m_j + (\boldsymbol{Bm})_j m_i \right] \left[(\boldsymbol{Bm})_l m_k + (\boldsymbol{Bm})_k m_l \right]$$

$$+ 4W_{15} \left[B_{ij} m_k (\boldsymbol{Bm})_l + B_{ij} m_l (\boldsymbol{Bm})_k \right.$$

$$\left. + B_{kl} m_j (\boldsymbol{Bm})_i + B_{kl} m_i (\boldsymbol{Bm})_j \right]$$

$$+ 4W_{25} \left\{ (I_1 \boldsymbol{B} - \boldsymbol{B}^2)_{ij} \left[(\boldsymbol{Bm})_l m_k + (\boldsymbol{Bm})_k m_l \right] \right.$$

$$\left. + (I_1 \boldsymbol{B} - \boldsymbol{B}^2)_{kl} \left[(\boldsymbol{Bm})_i m_j + (\boldsymbol{Bm})_j m_i \right] \right\}$$

$$+ 4W_{45} \left[m_i m_j m_k (\boldsymbol{Bm})_l + m_i m_j m_l (\boldsymbol{Bm})_k \right.$$

$$\left. + m_j m_k m_l (\boldsymbol{Bm})_i + m_i m_k m_l (\boldsymbol{Bm})_j \right]. \tag{39}$$

Consider for example the following strain energy density of the *neo-Hookean reinforcing model* (Merodio and Ogden, 2002),

$$W = \mu(I_1 - 3)/2 + F(I_4), \tag{40}$$

for an incompressible solid with one family of fibres, where F is a function of I_4 only and $\mu > 0$ is the initial shear modulus of the solid when $F \equiv 0$. Then the expressions above for the moduli reduce to

$$\mathcal{A}_{0jikl} = \mu \delta_{il} B_{jk} + 2F'(I_4) \delta_{il} m_j m_k + 4F''(I_4) m_i m_j m_k m_l. \tag{41}$$

Here, in addition to the major symmetries (28), we also find that $\mathcal{A}_{0jilk} = \mathcal{A}_{0jkli}$. It follows that we end up with 23 non-zero components, several of which are equal to one another. *In toto* there are 13 independent moduli.

Or take the case of a *plane pre-strain* in the $1, 2$ plane say, for an incompressible solid with only one family of fibres, lying in that plane. Then, in the coordinate system of the Eulerian principal axes,

$$\boldsymbol{B} = \begin{bmatrix} \lambda^2 & 0 & 0 \\ 0 & \lambda^{-2} & 0 \\ 0 & 0 & 1 \end{bmatrix}, \quad \boldsymbol{B}^{-1} = \begin{bmatrix} \lambda^{-2} & 0 & 0 \\ 0 & \lambda^2 & 0 \\ 0 & 0 & 1 \end{bmatrix} \tag{42}$$

and clearly

$$I_1 = I_2 = \lambda^2 + \lambda^{-2} + 1, \qquad I_3 = 1. \tag{43}$$

Also, $\boldsymbol{M} = (M_1, M_2, 0)$, say, with $M_1^2 + M_2^2 = 1$, so that

$$I_4 = \lambda^2 M_1^2 + \lambda^{-2} M_2^2 = m_1^2 + m_2^2, \qquad I_5 = \lambda^4 M_1^2 + \lambda^{-4} M_2^2 = \lambda^2 m_1^2 + \lambda^{-2} m_2^2. \tag{44}$$

Then we find the connection: $I_5 = (I_1 - 1)I_4 - 1$. Here there are thus only 2 independent invariants, and we can introduce the following function of two variables:

$$\hat{W}(I_1, I_4) = W\left(I_1, I_1, 1, I_4, (I_1 - 1)I_4 - 1\right). \tag{45}$$

11

That function allows for a reduced form of the moduli (Merodio and Ogden, 2002):

$$\mathcal{A}_{0jikl} = 2\hat{W}_1\delta_{il}B_{jk} + 2\hat{W}_4\delta_{il}m_jm_k + 4\hat{W}_{11}B_{ij}B_{kl}$$
$$+ 4\hat{W}_{44}m_jm_im_km_l + 4\hat{W}_{14}(B_{ij}m_km_l + B_{kl}m_im_j). \quad (46)$$

For an example in that category, take the *Mooney-Rivlin standard reinforcing model*,

$$W = C(I_1 - 3)/2 + D(I_2 - 3)/2 + E(I_4 - 1)^2/4, \quad (47)$$

where C, D and E are positive constants. Then $\hat{W}(I_1, I_4) = (C + D)(I_1 - 3) + E(I_4 - 1)^2/4$, and

$$\mathcal{A}_{0jikl} = (C + D)\delta_{il}B_{jk} + E(m_1^2 + m_2^2 - 1)\delta_{il}m_jm_k + 2Em_im_jm_km_l. \quad (48)$$

Finally, consider the following strain energy density used by Ciarletta et al. (2013) for modelling *skin tissue*, when seen as reinforced with a single family of fibres, oriented in $\mathcal{B}_0$ along the unit vector $\boldsymbol{M}$. It is given by

$$W = \frac{\mu}{2}(I_1 - 3) + \beta I_\alpha, \quad (49)$$

where $\mu > 0$ and $\beta > 0$ are constants, and the structural anisotropic invariant I_α is defined as

$$I_\alpha := \boldsymbol{M} \cdot \left[\boldsymbol{C} + \boldsymbol{C}^{-1} - 2\boldsymbol{I}\right]\boldsymbol{M} = (\lambda_\alpha - \lambda_\alpha^{-1})^2. \quad (50)$$

Here $\lambda_\alpha := (\boldsymbol{M} \cdot \boldsymbol{CM})^{\frac{1}{2}}$ represents the fibre stretch. For this model, the instantaneous moduli can again be computed from the formula (39), by noticing the connection

$$I_\alpha = (1 - I_1)I_4 + I_5 + I_2 - 2. \quad (51)$$

This is quite a long exercise however, and it is simpler to rely on the following formula:

$$\frac{\partial F_{\beta k}^{-1}}{\partial F_{i\alpha}} = -F_{\beta i}^{-1}F_{\alpha k}^{-1}, \quad (52)$$

which can be established by differentiating the identity $\boldsymbol{FF}^{-1} = \boldsymbol{I}$. The end result is that the corresponding moduli are

$$\mathcal{A}_{0jikl} = \mu\delta_{il}B_{jk} + 2\beta(\delta_{il}m_jm_k + \delta_{ik}F_{\alpha l}^{-1}M_\alpha F_{\beta j}^{-1}M_\beta$$
$$+ \delta_{jl}F_{\alpha i}^{-1}M_\alpha F_{\beta k}^{-1}M_\beta + \delta_{jk}F_{\alpha i}^{-1}M_\alpha F_{\beta l}^{-1}M_\beta). \quad (53)$$

3 Wave Propagation

In this section, we study small-amplitude wave propagation in infinite, homogeneous, incompressible, hyperelastic solids subject to large, static, homogeneous deformations. We look at the effect of anisotropy on the wave speed in initially isotropic solids and initially anisotropic (fibre-reinforced) tissues.

We take the axes of the Cartesian coordinate system in $\mathcal{B}$ to be aligned with the principal axes of deformation, that is we describe the pre-strain by

$$x_1 = \lambda_1 X_1, \qquad x_2 = \lambda_2 X_2, \qquad x_3 = \lambda_3 X_3, \tag{54}$$

where the λ's are the constant principal stretch ratios. Then the constraint of incompressibility dictates that a unit cube keeps its volume, so that $\lambda_1 \lambda_2 \lambda_3 = 1$.

Now, deriving the equations of *incremental motion* is a process similar to deriving those of incremental equilibrium (19); see Ogden (2007) for example. The end result is that they read

$$\Sigma_{ji,j} = \rho u_{i,tt}, \qquad u_{j,j} = 0, \tag{55}$$

where the components Σ_{ji} are given by (27) and ρ is the mass density per unit volume (ρ is constant in homogeneous bodies because of the internal constraint of incompressibility, see (2)). Let us solve the equations for a motion in the form of a *plane homogeneous wave*. For these, the mechanical displacement is written in all generality as

$$\boldsymbol{u} = \boldsymbol{a} f\left(\boldsymbol{n} \cdot \boldsymbol{x} - vt\right), \qquad \dot{p} = g\left(\boldsymbol{n} \cdot \boldsymbol{x} - vt\right), \tag{56}$$

where f and g are arbitrary single-variable functions, $\boldsymbol{n}$ is a unit vector in direction of *propagation*, $\boldsymbol{a}$ is a unit vector in direction of *polarisation*, and the real scalar v is the *speed*.

Then, the incremental incompressibility $(55)_2$ gives $a_j n_j f' = 0$, or

$$\boldsymbol{a} \cdot \boldsymbol{n} = 0. \tag{57}$$

In other words, the motion is *transverse*.

Next we note that the moduli $\mathcal{A}_{0jikl}$ and the Lagrange multiplier p are constants because the components $F_{i\alpha}$ of the deformation gradient $\boldsymbol{F}$ derived from (54) are constants themselves. It follows that the incremental equations of motion $(55)_1$ read

$$\mathcal{A}_{0jikl} a_l n_k n_j f'' - n_i g' = \rho v^2 f'' a_i \tag{58}$$

(note that the term involving p is $pu_{j,ij}$, which is zero by incremental incompressibility). Taking the product of this equation with a_i and using $\boldsymbol{a} \cdot \boldsymbol{n} = 0$, we arrive at the *secular equation*,

$$\rho v^2 = \mathcal{A}_{0jikl} a_i a_l n_j n_k, \tag{59}$$

which gives the wave speed in terms of the wave characteristics, the material properties and the pre-strain.

3.1 Strong Ellipticity for the Isotropic Matrix

From (59), we see that the speed is *real* when

$$\mathcal{A}_{0jikl} n_j n_k a_i a_l > 0, \quad \text{for all } \boldsymbol{a}, \boldsymbol{n} \text{ such that } \boldsymbol{a} \cdot \boldsymbol{a} = \boldsymbol{n} \cdot \boldsymbol{n} = 1, \ \boldsymbol{a} \cdot \boldsymbol{n} = 0. \tag{60}$$

This is the so-called *Strong Ellipticity* (SE) condition.

From here on we focus on wave propagation in a principal plane, by taking $\boldsymbol{n}$ in the (x_1, x_2) plane. Hence we have

$$\boldsymbol{n} = (n_1, n_2, 0), \quad \text{and either (i) } \boldsymbol{a} = (0, 0, 1) \text{ or (ii) } \boldsymbol{a} = (-n_2, n_1, 0), \tag{61}$$

where $n_1^2 + n_2^2 = 1$.

Recall that in *isotropic* materials, the principal axes of stress are aligned with the principal axes of strain. Then, in the (x_1, x_2, x_3) coordinate system, there are only 15 non-zero components of $\boldsymbol{\mathcal{A}_0}$ (Ogden, 1997). They are

$$\mathcal{A}_{0iijj}, \quad \mathcal{A}_{0ijij}, \quad \mathcal{A}_{0ijji}, \tag{62}$$

where there is no sum on the repeated indices.

Case (i): $\boldsymbol{a} = (0, 0, 1)$. Here SE reads $\mathcal{A}_{0j3k3} n_j n_k > 0$, i.e. $\mathcal{A}_{01313} n_1^2 + \mathcal{A}_{02323} n_2^2 > 0$ for all n_1, n_2. It follows that Strong Ellipticity imposes restrictions on the sign of some moduli, here

$$\mathcal{A}_{01313} > 0, \quad \mathcal{A}_{02323} > 0. \tag{63}$$

Case (ii): $\boldsymbol{a} = (-n_2, n_1, 0)$. Here SE can be written in the compact form

$$\alpha \, n_1^4 + 2\beta \, n_1^2 n_2^2 + \gamma \, n_2^4 > 0, \tag{64}$$

for all n_1, n_2, where

$$\alpha = \mathcal{A}_{01212}, \quad 2\beta = \mathcal{A}_{01111} + \mathcal{A}_{02222} - 2\mathcal{A}_{01122} - 2\mathcal{A}_{01221}, \quad \gamma = \mathcal{A}_{02121}. \tag{65}$$

Taking in turn $n_2 = 0$ and $n_1 = 0$ imposes $\alpha > 0$ and $\gamma > 0$. Then, taking $(n_2/n_1)^4 = \alpha/\gamma$ gives $\beta + \sqrt{\alpha\gamma} > 0$. Conversely, if the inequalities $\alpha > 0$, $\gamma > 0$, $\beta + \sqrt{\alpha\gamma} > 0$ are assumed, then

$$\alpha n_1^4 + 2\beta n_1^2 n_2^2 + \gamma n_2^4 > \alpha n_1^4 - 2\beta n_1^2 n_2^2 + \gamma n_2^4 = \left(\sqrt{\alpha}\, n_1^2 - \sqrt{\gamma}\, n_2^2\right) > 0, \quad (66)$$

and SE is satisfied. In conclusion, the SE condition is equivalent to

$$\alpha > 0, \qquad \gamma > 0, \qquad \beta + \sqrt{\alpha\gamma} > 0. \tag{67}$$

From now on, we assume that the *SE condition holds for the isotropic matrix.*

If for example the isotropic matrix is modelled by the Mooney–Rivlin material: $W = C(I_1 - 3)/2 + D(I_2 - 3)/2$, as in (47), then we find that

$$\alpha = \lambda_1^2 \left(C + D\lambda_3^2\right), \qquad \gamma = \lambda_2^2 \left(C + D\lambda_3^2\right), \qquad 2\beta = \alpha + \gamma. \tag{68}$$

Hence, SE reads: $C + D\lambda_3^2 > 0$, for all λ_3, so that we must have $C > 0$, $D > 0$. Similarly, if the matrix is modelled by the neo-Hookean model: $W = \mu(I_1 - 3)/2$, as in (40) and (49), then SE leads to $\mu > 0$.

3.2   Acoustic Tensor

Now we go back to the incremental equations of motion (58) for plane homogeneous waves. Multiplying the first equation by n_i and using (57) we obtain $g' = \mathcal{A}_{0jikl} n_i n_j n_k m_l f''$. Then we substitute back this expression for g' and drop the common factor f'' to arrive at

$$(\mathcal{A}_{0jikl} n_j n_k - \mathcal{A}_{0jpkl} n_j n_p n_k n_i) a_l = \rho v^2 a_i. \tag{69}$$

By introducing the symmetric *acoustic tensor* $\boldsymbol{Q}(\boldsymbol{n})$, with components

$$Q_{il}(\boldsymbol{n}) = \mathcal{A}_{0jikl} n_j n_k, \tag{70}$$

the equations above can be written in the compact form

$$[\boldsymbol{I} - \boldsymbol{n} \otimes \boldsymbol{n}]\boldsymbol{Q}(\boldsymbol{n})\boldsymbol{a} = \rho v^2 \boldsymbol{a}, \qquad \boldsymbol{a} \cdot \boldsymbol{n} = 0. \tag{71}$$

Note that the tensor $[\boldsymbol{I} - \boldsymbol{n} \otimes \boldsymbol{n}]\boldsymbol{Q}(\boldsymbol{n})$ is *not* symmetric. However, because the motion is transverse, we may write the equation above in the following equivalent form

$$[\boldsymbol{I} - \boldsymbol{n} \otimes \boldsymbol{n}]\boldsymbol{Q}(\boldsymbol{n})[\boldsymbol{I} - \boldsymbol{n} \otimes \boldsymbol{n}]\boldsymbol{a} = \rho v^2 \boldsymbol{a}, \qquad \boldsymbol{a} \cdot \boldsymbol{n} = 0. \tag{72}$$

By introducing $\bar{\boldsymbol{I}} = \boldsymbol{I} - \boldsymbol{n} \otimes \boldsymbol{n}$, the projection tensor onto the plane normal to $\boldsymbol{n}$, this reads as

$$\bar{\boldsymbol{Q}}(\boldsymbol{n})\boldsymbol{a} = \rho v^2 \boldsymbol{a}, \qquad \boldsymbol{a} \cdot \boldsymbol{n} = 0, \qquad \text{where} \quad \bar{\boldsymbol{Q}}(\boldsymbol{n}) = \bar{\boldsymbol{I}}\boldsymbol{Q}(\boldsymbol{n})\bar{\boldsymbol{I}} \qquad (73)$$

is a *symmetric tensor*. Note that this symmetrization of the acoustic tensor in constrained materials (including incompressible materials as here) is attributed to M.A. Hayes in the PhD thesis of N.H. Scott (see Scott and Hayes, 1985).

For any given direction of propagation $\boldsymbol{n}$, we now have (73), a 2D symmetric algebraic eigenvalue problem for determining ρv^2 and $\boldsymbol{a}$. Thanks to the symmetry of $\bar{\boldsymbol{Q}}$, we know that there are two mutually orthogonal eigenvectors $\boldsymbol{a}$ and $\boldsymbol{b}$, say, and that the two corresponding eigenvalues ρv_a^2 and ρv_b^2, say, must be real. They are obtained by solving the characteristic equation

$$\det[\bar{\boldsymbol{Q}}(\boldsymbol{n}) - \rho v^2 \boldsymbol{I}] = 0, \qquad (74)$$

which factorises into the product of ρv^2 by a quadratic. The eigenvalue $\rho v^2 = 0$ corresponds to eigenvector $\boldsymbol{n}$ and is discarded; the two other eigenvalues correspond to two purely transverse waves. When the eigenvalues coincide, we can superpose the two corresponding waves to form a *circularly-polarized wave*, which propagates along one of the so-called *acoustic axes*.

3.3 Example: Deformed Isotropic Material

First we treat the case of wave propagation when the anisotropy is *strain-induced* only. We take the deformed body to be made of an incompressible *isotropic Mooney–Rivlin material*, with strain-energy density $W = C(I_1 - 3)/2 + D(I_2 - 3)/2$, which is (47) when $E \equiv 0$.

First we consider waves travelling in a *principal plane* of pre-deformation, so that $\boldsymbol{n} = (\cos\theta, \sin\theta, 0)$ say, where θ is the angle of propagation in the principal plane with respect to the x_1-direction. Then the two transverse eigenvectors are $\boldsymbol{a} = (-\sin\theta, \cos\theta, 0)$ and $\boldsymbol{b} = (0, 0, 1)$, with corresponding eigenvalues
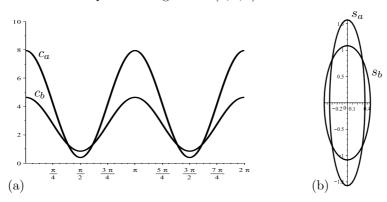
$$\rho v_a^2 = \lambda_1^2(C + D\lambda_3^2)\cos^2\theta + \lambda_2^2(C + D\lambda_3^2)\sin^2\theta,$$
$$\rho v_b^2 = \lambda_1^2(C + D\lambda_2^2)\cos^2\theta + \lambda_2^2(C + D\lambda_1^2)\sin^2\theta, \qquad (75)$$

respectively. To find these compact expressions we used the connections (68).

For our numerical calculations, we pick $\lambda_1 = 2$, $\lambda_2 = 0.45$, $\lambda_3 = (\lambda_1\lambda_2)^{-1}$ for the pre-stretch, and $C = 0.6\mu$, $D = 0.4\mu$ for the material parameters, where μ is the initial shear modulus (in Pa). In this example, the sinusoidal

16

variations of the speeds according to (75) are found to coincide twice over a half-period, indicating the presence of two acoustic axes in the deformed solid. To see this, we can either solve (75) for θ when $v_a = v_b$, or plot the variations of both speeds with θ and look for intersections, see Figure 4(a).

In wave acoustics, it is common to plot the *slowness surface*, because its shape is related to vibrational wavefronts which can be visualised experimentally (Musgrave, 1970; Wolfe, 1995). This is a spherical plot of the slowness $s := 1/v$ for each propagation direction $\boldsymbol{n}$. Hence for our waves propagating in the x_3-principal plane, the propagation vector is of the form $\boldsymbol{n} = (\cos\theta, \sin\theta, 0)$. For each angle of propagation θ, there are two slownesses $s_a := 1/v_a$ and $s_b := 1/v_b$ giving 2 points on the slowness surface: $(s_a, \theta, 0)$ and $(s_b, \theta, 0)$. Clearly, the two slowness sheets intersect in the directions of acoustic axes, see Figure 4(b) for the intersection of the slowness surface with the plane orthogonal to $(0, 0, 1)$.

(a)   (b)

Figure 4. Homogeneous plane wave travelling in a principal plane in a deformed (initially isotropic) Mooney–Rivlin material. (a) Variations of the non-dimensional speeds $c_a := \sqrt{\rho v_a^2/\mu}$ and $c_b := \sqrt{\rho v_b^2/\mu}$ with the angle of propagation θ measured with respect to the direction of greatest stretch. (b) Polar plot of the variations of the non-dimensional slownesses $s_a := 1/c_a$ and $s_b := 1/c_b$ with θ. The intersections of the plots point to the directions of 2 acoustic axes, along which circularly-polarised waves propagate.

Now for waves propagating *in any direction* $\boldsymbol{n}$, not necessarily in a principal plane, we specialise (70) and (73) to the Mooney–Rivlin strain energy function. We find that the reduced acoustic tensor reads

$$\bar{\boldsymbol{Q}}(\boldsymbol{n}) = C\,(\boldsymbol{n} \cdot \boldsymbol{B}\boldsymbol{n})\,\bar{\boldsymbol{I}} + D\bar{\boldsymbol{I}}\boldsymbol{B}^{-1}\bar{\boldsymbol{I}}. \tag{76}$$
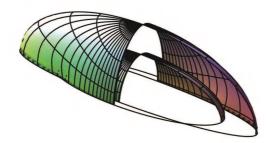
Hence here, it is perfectly possible to find explicit expressions for the wave

17

speeds and polarisation, simply by solving the eigenvalue problem for this tensor. In particular we can see straightaway that the polarisation vectors $\boldsymbol{a}$ and $\boldsymbol{b}$ are along the axes of the ellipsoidal section of the $\boldsymbol{x} \cdot \boldsymbol{B}^{-1}\boldsymbol{x} = 1$ ellipsoid by the plane normal to $\boldsymbol{n}$, as they are eigenvectors of both the $\bar{\boldsymbol{I}}\boldsymbol{B}^{-1}\bar{\boldsymbol{I}}$ and $\bar{\boldsymbol{I}}$ tensors. The corresponding speeds are then

$$\rho v_a^2 = C\left(\boldsymbol{n} \cdot \boldsymbol{B}\boldsymbol{n}\right) + D\left(\boldsymbol{a} \cdot \boldsymbol{B}^{-1}\boldsymbol{a}\right), \qquad \rho v_b^2 = C\left(\boldsymbol{n} \cdot \boldsymbol{B}\boldsymbol{n}\right) + D\left(\boldsymbol{b} \cdot \boldsymbol{B}^{-1}\boldsymbol{b}\right);$$
(77)

see Boulanger and Hayes (1992) for a full analysis of this problem.

To plot the entire slowness surface, we can take advantage of the graphical abilities of any mathematical/numerical package using a simple algorithm: Pick a propagation direction $\boldsymbol{n}$ with Cartesian components $\boldsymbol{n} = (\cos\theta\sin\phi, \sin\theta\sin\phi, \cos\phi)$, where θ and ϕ are its azimuthal and polar angles, respectively; Compute the corresponding reduced acoustic tensor $\bar{\boldsymbol{Q}}$ and its two eigenvalues ρv_a^2 and ρv_b^2; Plot the two points with spherical coordinates $(1/v_a, \theta, \phi)$ and $(1/v_b, \theta, \phi)$. Figure 5 illustrates the results of this algorithm for the same material and pre-strain parameter values used in Figure 4.

Figure 5. One quarter of a slowness surface composed of two sheets, each corresponding to the non-dimensional slownesses $s_a := \sqrt{\mu/(\rho v_a^2)}$ and $s_b := \sqrt{\mu/(\rho v_b^2)}$, using the same material and pre-strain parameter values used in Figure 4. The sheets are represented by a collection of points (s, θ, ϕ) in the spherical coordinate system, where θ and ϕ are the azimuthal and polar angles of propagation, respectively. The solid lines correspond to the intersection of the slowness surface sheets with the plane orthogonal to $(0, 0, 1)$.

3.4 Example: Deformed Anisotropic Material

To present a representative example, we focus here on a material reinforced by one family of parallel fibres behaving according to the Mooney–Rivlin standard reinforcing model (47).

Putting together Equations (70) and (73) for a general propagation direction $\boldsymbol{n}$, we arrive in that case at the following expression for the reduced acoustic tensor,

$$\bar{\boldsymbol{Q}}(\boldsymbol{n}) = \left[C\left(\boldsymbol{n} \cdot \boldsymbol{Bn}\right) + E\left(\boldsymbol{m} \cdot \boldsymbol{m} - 1\right)\left(\boldsymbol{m} \cdot \boldsymbol{n}\right)^2 \right] \bar{\boldsymbol{I}}$$
$$+ D\bar{\boldsymbol{I}} \boldsymbol{B}^{-1} \bar{\boldsymbol{I}} + 2E\left(\boldsymbol{m} \cdot \boldsymbol{n}\right)^2 \bar{\boldsymbol{I}} \boldsymbol{m} \otimes \bar{\boldsymbol{I}} \boldsymbol{m}. \quad (78)$$

This expression makes it clear that it not obvious at all now to find polarisation vectors as analytical eigenvectors for $\bar{\boldsymbol{Q}}$ in general, except in the special case where the direction of the fibres lies in a principal plane of deformation. Then, the two eigenvectors are clearly $\boldsymbol{b} := \boldsymbol{n} \times \boldsymbol{m}$ and $\boldsymbol{a} := \boldsymbol{n} \times \boldsymbol{b}$.

For an illustration, we take $C = 0.6\mu$, $D = 0.4\mu$, $E = 40\mu$ in (47), where μ (in Pa) can be seen as the initial shear modulus of the soft matrix. We let the fibres be originally at $45°$ between the X_1- and X_2-axes, i.e. $\boldsymbol{M} = (1/\sqrt{2}, 1/\sqrt{2}, 0)$. Then we subject the solid to the pre-strain (54), with $\lambda_1 = 1.4$, $\lambda_2 = 0.8$, $\lambda_3 = (\lambda_1\lambda_2)^{-1}$, so that $\boldsymbol{m} = \boldsymbol{FM}$ is at angle $\tan^{-1}\left[\lambda_2 \sin\alpha/(\lambda_1 \cos\alpha)\right] \simeq 27.4°$ with the x_1-axis, which gives the direction of the fibres in the deformed configuration.

By taking $\boldsymbol{n} = (\cos\theta, \sin\theta, 0)$ and varying θ, we obtain the dispersion curves and slowness surface principal sections of Figure 6. Clearly, the introduction of fibres brings in a more colourful behaviour, as their presence is strongly felt in the variations of c_a and s_a for the wave polarised in the principal plane. In particular we see that this transverse wave travels at its slowest in the direction perpendicular to the fibres. The speed c_a is at a local minimum when the corresponding wave travels in the direction of the fibres, and reaches its maximum at an intermediate angle. Meanwhile the speed c_b of the wave polarised along the x_3-direction has more regular (sinusoidal) variations. Although the variation of these speeds could be studied analytically, we do not pursue this avenue here, as they are attached to the special case of principal plane propagation. In general, it is better to turn to a numerical treatment of the eigenvalues, following the algorithm presented in the previous subsection. For the present case study, it leads to the slowness surface depicted in Figure 7.
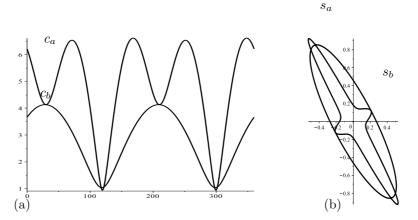
Figure 6. Homogeneous plane wave travelling in a principal plane in a deformed (initially anisotropic) Mooney–Rivlin material reinforced with one family of parallel fibres. (a) Variations of the non-dimensional speeds $c_a := \sqrt{\rho v_a^2/\mu}$ and $c_b := \sqrt{\rho v_b^2/\mu}$ with the angle of propagation θ measured with respect to the direction of greatest stretch. Here the fibres are in the principal plane, originally aligned in the direction $\theta = 45°$. (b) Polar plot of the variations of the non-dimensional slownesses $s_a := 1/c_a$, $s_b := 1/c_b$ with θ.

4 Surface Stability

Now we move on from the study of infinitesimal waves in unbounded (infinite) deformed solids to the study of small-amplitude perturbations in a deformed *bounded* media reinforced with fibres. The complexity of the analysis increases dramatically and we must be careful to take a step-by-step approach to tackling this complexity. Hopefully then, each result we establish along the way can serve as a benchmark or limiting case for the next degree of difficulty.

Hence we look at the simplest boundary problem possible, that of a *semi-infinite solid* limited by a plane. Since there is no characteristic length in a half-space geometry, the results ought to be *non-dispersive* (independent of a wavelength). Then we focus on small-amplitude *static wrinkles* instead of waves, again to decrease the number of parameters. To fix the ideas, we select *simple shear* as the base large pre-strain, as it described by a single kinematic parameter, the amount of shear K, say, and we imagine that it takes place in planes parallel to the free surface. Thus we take the solid to fill the half-space $X_2 \geq 0$ in the reference configuration. We subject it to
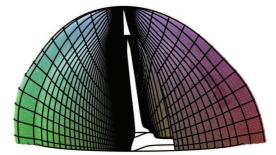
Figure 7. One quarter of a slowness surface composed of two sheets, each corresponding to the non-dimensional slownesses $s_a := \sqrt{\mu/(\rho v_a^2)}$ and $s_b := \sqrt{\mu/(\rho v_b^2)}$, using the same material and pre-strain parameter values used in Figure 6. The sheets are represented by a collection of points (s, θ, ϕ) in the spherical coordinate system, where θ and ϕ are the azimuthal and polar angles of propagation, respectively. The solid lines correspond to the intersection of the slowness surface sheets with the plane orthogonal to $(0, 0, 1)$.

the simple shear

$$x_1 = X_1 + KX_2, \qquad x_2 = X_2, \qquad x_3 = X_3, \tag{79}$$

so that it fills the region $x_2 \geq 0$ in the deformed configuration, and the planes $X_2 = 0$ and $x_2 = 0$ are assumed to be free of traction. We call $\boldsymbol{E}_i$ and $\boldsymbol{e}_i$ $(i = 1, 2, 3)$ the unit vectors along the X_i- and x_i-axes, respectively. Then, in the $\boldsymbol{E}_i \otimes \boldsymbol{e}_j$ and $\boldsymbol{e}_i \otimes \boldsymbol{e}_j$ bases, respectively, the deformation gradient $\boldsymbol{F} = \partial \boldsymbol{x}/\partial \boldsymbol{X}$ and the left Cauchy–Green deformation gradient $\boldsymbol{B} = \boldsymbol{F}\boldsymbol{F}^T$ have components

$$\boldsymbol{F} = \begin{bmatrix} 1 & K & 0 \\ 0 & 1 & 0 \\ 0 & 0 & 1 \end{bmatrix}, \qquad \boldsymbol{B} = \begin{bmatrix} 1 + K^2 & K & 0 \\ K & 1 & 0 \\ 0 & 0 & 1 \end{bmatrix}. \tag{80}$$

We expect that as the magnitudes of the strains increase during a large simple shear, there will be directions of severe compression developing for some line elements and eventually, at a *critical amount of shear* K_{cr}, say, the surface will buckle and let wrinkles appear. For the solid, we consider in turn an isotropic neo-Hookean model, and then a soft neo-Hookean matrix reinforced with a single family of stiffer parallel fibres lying in the planes parallel to the free surface.

In other words, our ultimate goal in this section is to model the physical behaviours reported in Figure 1.

4.1 Surface Instability for a Sheared Isotropic Material

We start off by studying the onset of wrinkles in a sheared isotropic neo-Hookean material, with strain-energy density

$$W = \mu(I_1 - 3), \tag{81}$$

where $\mu > 0$ is the shear modulus.

Biot (1963) showed that surface instability occurs for this material when the following *wrinkling condition* is met

$$\lambda_1^2 \lambda_3 = \sigma_0, \tag{82}$$

where $\sigma_0 \simeq 0.296$ is the real root of the cubic $\sigma^3 + \sigma^2 + 3\sigma - 1 = 0$. Here it is assumed that the free surface is parallel to a principal plane of pre-strain. In that plane, $\lambda_1 < 1$ and $\lambda_3 \geq 1$ are the principal stretches and $\lambda_2 = (\lambda_1 \lambda_3)^{-1}$ is the principal stretch in the direction normal to the surface (the depth). The wrinkles decay exponentially with depth and have sinusoidal variations along the surface, with their front running parallel to the principal Eulerian axis where λ_3 occurs. That is, they are parallel to the direction of greatest tension and thus, orthogonal to the direction of greatest compression.

The simple shear described by (79) is a *plane strain deformation*, such that

$$\lambda_1 = \lambda, \qquad \lambda_2 = 1, \qquad \lambda_3 = \lambda^{-1}, \tag{83}$$

say. Then Biot's wrinkling condition clearly gives the *critical stretch of compression* as $\lambda_{\text{cr}} = \sigma_0 \simeq 0.296$, and thus the critical stretch of extension as $\lambda_3 = \sigma_0^{-1} \simeq 3.38$. We conclude that the wrinkles appear when the solid is compressed by 71%, or equivalently, when it is stretched by 238%.

This is quite an extreme deformation for a soft solid. To connect it with the kinematics of simple shear, we recall the links between the principal stretches and the amount of shear (Ogden, 1997)

$$K = \lambda_3 - \lambda_1, \qquad \lambda_3 = K/2 + \sqrt{1 + K^2/4}, \tag{84}$$

and that the *angle of shear* is $\tan^{-1} K$ (when the solid is not sheared, this angle is zero; when it is infinitely sheared, this angle tends to 90° as a limit).

So here, surface instability in a sheared isotropic neo-Hookean material occurs when

$$K = K_{\text{cr}} = \sigma_0^{-1} - \sigma_0 \simeq 3.09, \qquad \text{and} \qquad \tan^{-1} K = \tan^{-1} K_{\text{cr}} \simeq 72.0°. \tag{85}$$

This is a very large shear, as seen Figure 8. These values go a long way to explaining why the surface of the sheared silicone in Figure 1(a) remains stable, as the angle of shear there is clearly less than 72°.
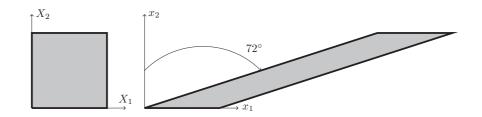

Figure 8. The amount of shear required to reach surface instability for an isotropic neo-Hookean half-space is $K_{cr} = 3.09$, which represents an enormous strain, as shown here.

However large, it is nonetheless possible to create a homogeneous pre-strain of that magnitude in a soft solid, and to observe the appearance of surface instability when a critical threshold is reached. To produce the experiment photographed in Figure 9, we filled up the third of a four-sided plexiglass box with commercial gelatine. The four connecting edges of the box are hinged so that a large homogeneous 'shear-box' deformation is possible, which can be decomposed into the combination of a simple shear and a tri-axial stretch (Stolz, 2010). At a very large amount of pre-strain, we see small-amplitude wrinkles form on the surface, and they are aligned with the long diagonal of the deformed shear-box, which is in the direction of largest stretch.

To complete the picture, we can ask ourselves an additional question: Do the wrinkles always occur along the direction of greatest stretch? Indeed, Biot (1963) only studied wrinkles appearing along a principal direction, at a certain degree of compression. But what if 'non-principal' wrinkles had appeared prior to reaching his critical state of deformation? Intuition and the observation of Figure 9 tell us that 'principal' wrinkles should be the general case, but we must keep in mind that wrinkling in a principal direction is not necessarily the sole outcome of a surface instability analysis (Gower and Destrade, submitted) nor of experiments: for instance, 'oblique' buckling wrinkles have been observed in polymeric strips (Wang et al., 2011) or in meta-sedimentary rocks (Meere et al., 2013).

Thankfully, answering this question for the neo-Hookean surface instability problem is easy, as we can rely on the works of Flavin (1963). He
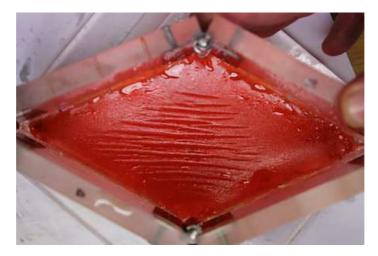
Figure 9. Large homogenous strain of soft gelatine in a shear-box apparatus, up to the critical threshold of surface instability, as indicated by the formation of small-amplitude wrinkles aligned with the long diagonal.

showed that wrinkles develop parallel to the direction making an angle θ with the principal direction of strain associated with the largest stretch λ_3 when the following *wrinkling condition* is met

$$\lambda_1^2 \lambda_3^2 (\lambda_1^2 \cos^2 \theta + \lambda_3^2 \sin^2 \theta) = \sigma_0^2. \tag{86}$$

In the plane strain situation above, this condition reads as

$$\lambda^4 \cos^2 \theta - \lambda^2 \sigma_0^2 + \sin^2 \theta = 0. \tag{87}$$

This quadratic in $\lambda^2 < 1$ has real roots provided θ is in the range $-\theta_0 \leq \theta \leq \theta_0$, where $\theta_0 = (1/2) \sin^{-1} \sigma_0^2 \simeq 2.51°$. In that narrow range, λ reaches a maximum of 0.296 when $\theta = 0°$, indicating that wrinkles take place at that level of compression and are aligned with the direction of greatest stretch. We expect this situation to be completely different for anisotropic materials, because the fibres and their orientation should play a major role in the onset of wrinkles, see Figure 1(b).

4.2   Surface Instability for a Sheared Anisotropic Material

Now we introduce one family of parallel fibres, orientated along the unit vector $\boldsymbol{M}$ with components

$$\boldsymbol{M} = \cos \varPhi \boldsymbol{E}_1 + \sin \varPhi \boldsymbol{E}_3 \tag{88}$$

in the reference configuration, where Φ is the angle between the direction of shear and the fibres. Simple shear is a homogeneous deformation and so, using (80), we see that M is transformed into $m = FM$ in the current configuration,

$$m = (\cos\Phi + K\sin\Phi)e_1 + \sin\Phi\,e_3. \tag{89}$$

It follows that the anisotropic invariant $I_4 \equiv m \cdot m$ is given by

$$I_4 = 1 + K\sin 2\Phi + K^2\sin^2\Phi. \tag{90}$$

Recall that I_4 is the squared stretch in the fibre direction: if $I_4 \geq 1$ then the fibres are in extension, if $I_4 \leq 1$ then they are in compression. For our constitutive assumptions, we move on from the isotropic neo-Hookean material to the *standard reinforcing neo-Hookean material*, a subcase of (47):

$$W = \mu(I_1 - 3)/2 + E(I_4 - 1)^2/4. \tag{91}$$

In that case, it is a simple exercise to show that the corresponding Cauchy stress tensor σ is

$$\sigma = -pI + \mu B + E(I_4 - 1)m \otimes m, \tag{92}$$

where p is the Lagrange multiplier introduced by the constraint of incompressibility. Its value is found by imposing that the surface $x_2 = 0$ be free of traction: $\sigma_{22} = 0$, which gives $p = \mu$.

Thus, the pre-stress required to maintain the large static simple shear is

$$\sigma = \mu(B - I) + E(I_4 - 1)m \otimes m, \tag{93}$$

showing clearly that the directions of principal stress and of principal strain do not coincide in general (except of course in the special cases where m is aligned with principal directions of strain).

Finally, we note that according to the Appendix, the quantity $2E/3\mu$ is a measure of the stiffness of the fibres compared to that of the soft matrix: if it is greater than 1, then the fibres are stiffer than the matrix, at least in a tensile, infinitesimal, tensile test.

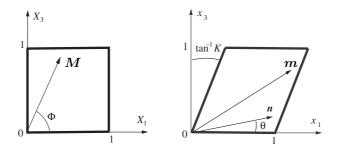Now we seek a perturbation solution in the following form,

$$\{u, \dot p\} = \{U(kx_2), ikP(kx_2)\}e^{ik(\cos\theta x_1 + \sin\theta x_3)}, \tag{94}$$

where k is the "wave"-number and U, P are functions of kx_2 alone. This form describes wrinkles in the deformed configuration with sinusoidal variations in the direction of $n = (\cos\theta, \sin\theta, 0)$, and depth variations according

to the amplitude functions U and P, to be determined later. Then, according to (27), the components Σ_{ji} for the incremental traction are of a similar form,

$$\Sigma_{ji} = \mathrm{i}k S_{ji}(kx_2)\mathrm{e}^{\mathrm{i}k(\cos\theta x_1 + \sin\theta x_3)}, \tag{95}$$

say, where the amplitude functions S_{ij} are to be determined. All the kinematical quantities of interest are represented in Figure 10.

Figure 10. Simple shear of a unit cuboid in the boundary of a half-space by amount K. The face shown is parallel to the free surface. The solid is reinforced with a family of parallel fibres aligned in the direction of $\boldsymbol{M} = (\cos\Phi, \sin\Phi, 0)$ in the reference configuration and of $\boldsymbol{m} = \boldsymbol{F}\boldsymbol{M}$ in the current configuration. The unit vector $\boldsymbol{n} = (\cos\theta, \sin\theta, 0)$ in the current configuration is orthogonal to the wavefront of wrinkles which may develop if the shear is severe enough.

By relying on a systematic procedure devised by Chadwick (1997), we can eliminate P and write the governing equations (19) as a first-order linear ordinary differential system. This is known as the *Stroh formulation* of the problem (Stroh, 1962),

$$\begin{bmatrix} \boldsymbol{U}' \\ \boldsymbol{S}' \end{bmatrix} = \mathrm{i}\boldsymbol{N} \begin{bmatrix} \boldsymbol{U} \\ \boldsymbol{S} \end{bmatrix}, \text{ where } \boldsymbol{U} := \begin{bmatrix} U_1 \\ U_2 \\ U_3 \end{bmatrix}, \quad \boldsymbol{S} := \begin{bmatrix} S_{21} \\ S_{22} \\ S_{23} \end{bmatrix}, \quad \boldsymbol{N} := \begin{bmatrix} \boldsymbol{N}_1 & \boldsymbol{N}_2 \\ \boldsymbol{N}_3 & \boldsymbol{N}_1 \end{bmatrix}, \tag{96}$$

and the prime denotes differentiation with respect to the argument kx_2. Here the symmetric 3×3 matrices $\boldsymbol{N}_1$, $\boldsymbol{N}_2$, $\boldsymbol{N}_3$ are given by

$$-\boldsymbol{N}_1 = \begin{bmatrix} 0 & \cos\theta & 0 \\ \cos\theta & 0 & \sin\theta \\ 0 & \sin\theta & 0 \end{bmatrix}, \quad \boldsymbol{N}_2 = \begin{bmatrix} 1/\mu & 0 & 0 \\ 0 & 0 & 0 \\ 0 & 0 & 1/\mu \end{bmatrix}, \quad -\boldsymbol{N}_3 = \begin{bmatrix} \eta & 0 & \kappa \\ 0 & \nu & 0 \\ \kappa & 0 & \chi \end{bmatrix},$$

with

$$\eta = (\mathcal{A}_{01111} + 3\mu)\cos^2\theta + 2\mathcal{A}_{01131}\cos\theta\sin\theta + \mathcal{A}_{03131}\sin^2\theta,$$
$$\nu = \mathcal{A}_{01212}\cos^2\theta + 2\mathcal{A}_{01232}\cos\theta\sin\theta + \mathcal{A}_{03232}\sin^2\theta - \mu,$$
$$\chi = \mathcal{A}_{01313}\cos^2\theta + 2\mathcal{A}_{01333}\cos\theta\sin\theta + (\mathcal{A}_{03333} + 3\mu)\sin^2\theta,$$
$$\kappa = \mathcal{A}_{01113}\cos^2\theta + (2\mathcal{A}_{01133} + 3\mu)\cos\theta\sin\theta + \mathcal{A}_{03133}\sin^2\theta,$$

and the components of $\mathcal{A}_{\mathbf{0}}$ are given explicitly by (41), with $F' = 2E(I_4 - 1)$ and $F'' = 2E$. Notice how all the "anisotropy" information is located in the N_3 sub-matrix. For details of this derivation, see Destrade et al. (2008).

The system (96) can be written in compact form as

$$\boldsymbol{\xi}' = \mathrm{i}\boldsymbol{N}\boldsymbol{\xi}, \qquad \text{where} \qquad \boldsymbol{\xi} := [\boldsymbol{U}, \boldsymbol{S}]^T, \tag{97}$$

is the Stroh displacement–traction vector, a function of the dimensionless quantity kx_2. Its solution is clearly an exponential:

$$\boldsymbol{\xi}(kx_2) = \left[\boldsymbol{U}^0, \boldsymbol{S}^0\right]^T \mathrm{e}^{\mathrm{i}kqx_2}, \tag{98}$$

say, where $\boldsymbol{U}^0, \boldsymbol{S}^0$ are constant vectors and q is an eigenvalue of $\boldsymbol{N}$. In effect we now have to solve an *eigenvalue problem* for the Stroh matrix $\boldsymbol{N}$:

$$(\boldsymbol{N} - q\boldsymbol{I})\boldsymbol{\xi}^0 = \mathbf{0}. \tag{99}$$

The associated characteristic equation $\det(\boldsymbol{N} - q\boldsymbol{I}) = 0$ is a *cubic* in q^2,

$$q^6 - \left(2 - \frac{\chi + \eta}{\mu}\right)q^4 + \left(1 + \frac{\nu - 2\epsilon}{\mu} + \frac{\chi\eta - \kappa^2}{\mu^2}\right)q^2 + \frac{\epsilon(\mu + \nu)}{\mu^2} = 0, \tag{100}$$

where the quantity ϵ is defined by

$$\epsilon := \chi\cos^2\theta - 2\kappa\cos\theta\sin\theta + \eta\sin^2\theta. \tag{101}$$

Here we focus on complex roots to the bicubic, because we are looking for solutions with amplitudes decaying with depth–real roots would lead to inadequate sinusoidal non-decaying depth variations. Since the polynomial characteristic equation has real coefficients, the complex roots come in pairs of complex conjugate numbers. Specifically, out of the six possible complex roots, we can only keep those three satisfying $\mathrm{Im}\, q > 0$; see the form of the solution in (98). These three adequate roots q_1, q_2, q_3 allow us to find three independent solutions to the differential system, which we combine to form its general solution as

$$\boldsymbol{\xi}(kx_2) = c_1\boldsymbol{\xi}^{(1)}\mathrm{e}^{\mathrm{i}q_1 kx_2} + c_2\boldsymbol{\xi}^{(2)}\mathrm{e}^{\mathrm{i}q_2 kx_2} + c_3\boldsymbol{\xi}^{(3)}\mathrm{e}^{\mathrm{i}q_3 kx_2}, \tag{102}$$

where the c_i are scalar constants and the $\boldsymbol{\xi}^{(i)}$ are the eigenvectors. We write this general solution as

$$\boldsymbol{\xi}(kx_2) = \left[\boldsymbol{\xi}^{(1)}|\boldsymbol{\xi}^{(2)}|\boldsymbol{\xi}^{(3)}\right] \left\langle e^{iqkx_2} \right\rangle \begin{bmatrix} c_1 \\ c_2 \\ c_3 \end{bmatrix}, \tag{103}$$

where we adopted the notation $\left\langle e^{iqkx_2} \right\rangle := \operatorname{diag}\left(e^{iq_1kx_2}, e^{iq_2kx_2}, e^{iq_3kx_2}\right)$. We re-write it even more compactly as

$$\boldsymbol{\xi}(kx_2) = \begin{bmatrix} \boldsymbol{A} \\ \boldsymbol{B} \end{bmatrix} \left\langle e^{iqkx_2} \right\rangle \boldsymbol{c}, \tag{104}$$

where $\boldsymbol{A}$ ($\boldsymbol{B}$) is the 3×3 matrix made with the top (bottom) three rows of $\left[\boldsymbol{\xi}^{(1)}|\boldsymbol{\xi}^{(2)}|\boldsymbol{\xi}^{(3)}\right]$. Hence now

$$\boldsymbol{U}(kx_2) = \boldsymbol{A} \left\langle e^{iqkx_2} \right\rangle \boldsymbol{c}, \qquad \boldsymbol{S}(kx_2) = \boldsymbol{B} \left\langle e^{iqkx_2} \right\rangle \boldsymbol{c}. \tag{105}$$

Now that we have the general solution, we can solve the boundary value problem, which states that there should be no incremental traction on the free surface, that is

$$\boldsymbol{S}(0) = \boldsymbol{0}. \tag{106}$$

According to $(105)_2$, this is possible for non-trivial $\boldsymbol{c}$ only when $\det \boldsymbol{B} = 0$, which is the *bifurcation criterion*. However this is not expressed in the most optimal way. In particular, computing numerically the eigenvalues and corresponding linearly independent eigenvectors of $\boldsymbol{N}$ is quite demanding from a computational point of view. For certain cases, the complex matrix $\boldsymbol{B}$ becomes ill-conditioned and finding numerically for which values of K it becomes singular is not an easy task at all. So we turn to a much more efficient method, based on the notion of mechanical impedance.

We remark that it follows from (105) that $\boldsymbol{c} = \left\langle e^{-iqkx_2} \right\rangle \boldsymbol{A}^{-1} \boldsymbol{U}(kx_2)$, and that

$$\boldsymbol{S}(kx_2) = i\boldsymbol{Z}\boldsymbol{U}(kx_2), \qquad \text{where} \quad \boldsymbol{Z} := -i\boldsymbol{B}\boldsymbol{A}^{-1} \tag{107}$$

is the so-called *surface impedance matrix*. Clearly, the matrix $\boldsymbol{Z}$ is constant (independent of x_2). Also, it is singular, because the boundary condition (106) can only be satisfied for a nontrivial surface displacement $\boldsymbol{U}(0)$ when

$$\det \boldsymbol{Z} = 0. \tag{108}$$

Finally, it can be shown (e.g., Shuvalov, 2000; Mielke and Fu, 2004) that $\boldsymbol{Z}$ is Hermitian so that it is of the form

$$\boldsymbol{Z} = \begin{bmatrix} Z_1 & Z_4 + iZ_5 & Z_6 + iZ_7 \\ Z_4 - iZ_5 & Z_2 & Z_8 + iZ_9 \\ Z_6 - iZ_7 & Z_8 - iZ_9 & Z_3 \end{bmatrix}, \tag{109}$$

where the Z_i are real constants.

Then, using (107), the governing equations (97) read as

$$\boldsymbol{U}' = \mathrm{i}\boldsymbol{N}_1\boldsymbol{U} + \mathrm{i}\boldsymbol{N}_2\boldsymbol{S} = \mathrm{i}\boldsymbol{N}_1\boldsymbol{U} + \boldsymbol{N}_2\boldsymbol{Z}\boldsymbol{U}, \tag{110}$$

$$\boldsymbol{S}' = \mathrm{i}\boldsymbol{N}_3\boldsymbol{U} + \mathrm{i}\boldsymbol{N}_1\boldsymbol{S} = \mathrm{i}\boldsymbol{N}_3\boldsymbol{U} + \boldsymbol{N}_1\boldsymbol{Z}\boldsymbol{U} = -\mathrm{i}\boldsymbol{Z}\boldsymbol{U}'. \tag{111}$$

Substitute the first line into the second to end up with

$$\boldsymbol{Z}\boldsymbol{N}_2\boldsymbol{Z} + \mathrm{i}\boldsymbol{Z}\boldsymbol{N}_1 - \mathrm{i}\boldsymbol{N}_1\boldsymbol{Z} + \boldsymbol{N}_3 = \boldsymbol{0}, \tag{112}$$

an algebraic *Riccati matrix equation.* Because the $\boldsymbol{N}_i$ are real symmetric matrices and $\boldsymbol{Z}$ is Hermitian, writing separately the real and imaginary parts of this equation yields nine real quadratic equations for the Z_i of (109). Together with the traction-free boundary condition (106), we have an algebraic system of 10 equations for the 10 unknowns $Z_1, Z_2, \ldots, Z_9$ and K. It goes as follows

$$2\mu\cos\theta Z_5 - Z_1^2 - Z_6^2 - Z_7^2 + \mu\eta = 0,$$
$$\mu\sin\theta Z_7 - Z_1 Z_4 - Z_6 Z_8 - Z_7 Z_9 = 0,$$
$$\mu\sin\theta Z_5 - \mu\cos\theta Z_9 - Z_1 Z_6 - Z_3 Z_6 + \mu\kappa = 0,$$
$$\mu\cos\theta(Z_1 - Z_2) + \mu\sin\theta Z_6 + Z_1 Z_5 - Z_6 Z_9 + Z_7 Z_8 = 0,$$
$$2\mu\cos\theta Z_5 - 2\mu\sin\theta Z_9 + Z_5^2 + Z_9^2 + Z_4^2 + Z_8^2 - \mu\nu = 0,$$
$$\mu\cos\theta Z_7 + Z_5 Z_7 + Z_3 Z_8 + Z_4 Z_6 = 0,$$
$$\mu\cos\theta Z_8 - \mu\sin\theta Z_4 - Z_1 Z_7 - Z_3 Z_7 = 0,$$
$$\mu\cos\theta Z_6 - \mu\sin\theta(Z_2 - Z_3) - Z_3 Z_9 - Z_4 Z_7 + Z_5 Z_6 = 0,$$
$$2\mu\sin\theta Z_9 + Z_7^2 + Z_3^2 + Z_6^2 - \mu\chi = 0,$$
$$Z_1 Z_2 Z_3 - Z_1 Z_8^2 - Z_1 Z_9^2 - Z_2 Z_6^2 - Z_2 Z_7^2 - Z_3 Z_4^2 - Z_3 Z_5^2$$
$$+ 2Z_4 Z_6 Z_8 + 2Z_4 Z_7 Z_9 - 2Z_5 Z_6 Z_9 + 2Z_5 Z_7 Z_8 = 0. \tag{113}$$

The system is non-linear and may thus have several solutions, but there is only one for which $\boldsymbol{Z}$ is positive semi-definite, corresponding to the decaying solution (Fu and Mielke, 2002). This system provides us with the following algorithm for solving the bifurcation criterion.

We prescribe the material parameters: μ the shear modulus, E the fibre modulus, and Φ the angle of the fibres. Then we fix θ, the wrinkles angle. Then, the only remaining unknowns are the solutions, if they exist, to the system above.

We start at $K = 0$ (no shear) and increment slowly this quantity, until it reaches a value K_{cr} at which the system has a solution. If it exists, then

that is the point at which the bifurcation criterion is met. Of course, it could be that wrinkles have appeared earlier, at a lower amount of shear, for another θ. We must thus vary θ from $0°$ to $180°$ and find the angle θ^* for which the amount of shear K_{cr} is minimal, $K_{\text{cr}} = K^*$, say, which corresponds to the earliest onset of wrinkling in an oblique direction.

At the end of this process, we have access to the critical amount of shear K^* for a given material. It tells us how much the body can be sheared before instability, and gives us the deformation gradient and the current orientation of the fibres. With the value of θ^* we know how the wrinkles are oriented with respect to the fibres. With the value of $\boldsymbol{Z}$, we can solve $\boldsymbol{ZU}(0) = \boldsymbol{0}$ for $\boldsymbol{U}(0)$ to find the shape of the wrinkles on the free surface (up to an arbitrary multiplicative parameter: recall that this is a linearised stability analysis). In fact, by solving numerically the differential equation (110) we can find the variations of the full incremental field displacements with depth, and then use (107) to obtain those of the traction field.

Now if we want to investigate the effect of the orientation of the fibres with respect to the direction of shear, we can vary Φ and eventually obtain a $K^* - \Phi$ stability plot. Then we can vary the value of E/μ to investigate the effect of the relative strength of the fibres compared to the soft matrix. It transpires that those later curves are quite tricky to acquire due the following reason.

At $\Phi = 0$, the critical amount of shear is very close to the value $\sigma_0^{-1} - \sigma_0 \simeq 3.09$ found in (85) for the isotropic neo-Hookean half-space ($E \equiv 0$). Then as Φ is increased, a smooth increase in K^* follows. Hence for each increase in Φ, the natural inclination is to look for the next K^* in the neighborhood of the previous one. However, the search should always start from $K = 0$ instead, because as it happens, the $K^* - \Phi$ stability plot is discontinuous: at a certain angle Φ_0, the material stops being made more stable by the fibres and instead, becomes unstable at a very low value of K^*. This is illustrated by the example in Figure 11, where the situation is summarised in the caption. In that example it is found that when $E/\mu = 10.0$, and the fibres are originally at an angle $\Phi = 106°$, then the surface of the half-space buckles as soon as K reaches $K^* \simeq 0.052$, a tiny amount of shear. In the current configuration, the direction of the fibres is found from (89) as $103°$. The normal to the wrinkles-front is oriented at an angle $\theta^* \simeq 107°$, which means that the wrinkles are almost at right-angle with the fibres, a nice agreement with the observation in the simple experiment of Figure 1(b).

In Figure 12 we collect the $K^* - \Phi$ plots for different values of E/μ. The Appendix shows that in the linear regime of a tensile test along the fibres, the Young modulus of the material is $3\mu + 2E$, so that in a sense, $2E/3\mu$ represents the fibre-to-matrix stiffness ratio. For the figure we take
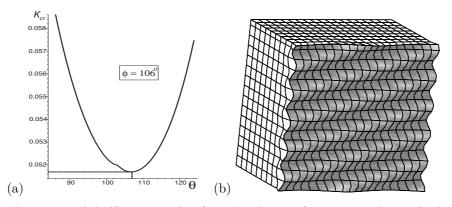
30

Figure 11. A half-space made of neo-Hookean soft matrix with standard reinforcement can buckle very early in simple shear. Here the E/μ ratio is equal to 10.0. When the fibres are originally at $\Phi = 106°$ to the shear direction, wrinkles appear at $K^* \simeq 0.052$, with the normal to the wrinkle front at $\theta^* \simeq 107°$ from the wrinkles. (a) The $K_{\text{cr}} - \theta$ curve, leading to the determination of the critical values K^* and θ^* (intersection of the dashed lines). (b) The corresponding surface buckling pattern, with wrinkles forming at right angle to the fibres.

$E/\mu = 1.0$ (fibres softer than the matrix), 2.0, 4.0, 8.0, 16.0 (fibres stiffer than the matrix). We find that when the fibres are originally more or less oriented along the direction of shear, the stability is enhanced compared to the non-reinforced case and $K^* > 3.09$. Then, as mentioned earlier for the $E/\mu = 10.0$ case, a dramatic drop in the value of K^* occurs at some angle Φ, whose value decreases as E/μ increases. In other words, the stiffer the fibres, the wider the range of early surface instability in shear.

4.3   Surface Instability for Another Sheared Anisotropic Material

Finally, we consider materials with a neo-Hookean soft matrix, also reinforced by one family of fibres, but this time modelled according to the strain energy density (49). According to Ciarletta et al. (2011, 2013), this constitutive modelling ensures *strong convexity* of the whole tissue (matrix and fibres) in planar deformations, in contrast with standard models of fibre reinforcement.

Again, it is easy to find the Lagrange multiplier p such that the surface $x_2 = 0$ is free of traction as $p = \mu$. We then find that the Cauchy pre-stress
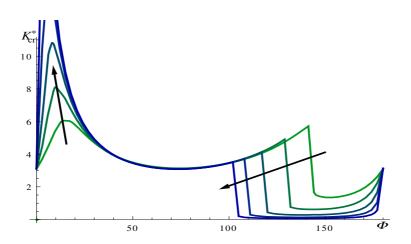
31

Figure 12. Bifurcation plots for surface instability of a neo-Hookean soft matrix with standard reinforcement in simple shear: Critical amount of shear K^* vs orientation Φ of the fibres in the reference configuration, for $E/\mu = 1.0, 2.0, 4.0, 8.0, 16.0$ (increasing values indicated by arrows).

required to maintain the large static simple shear is

$$\boldsymbol{\sigma} = \mu(\boldsymbol{B} - \boldsymbol{I}) + 2\beta(\boldsymbol{FM} \otimes \boldsymbol{FM} - \boldsymbol{F}^{-T}\boldsymbol{M} \otimes \boldsymbol{F}^{-T}\boldsymbol{M}), \qquad (114)$$

where $\boldsymbol{F}$ and $\boldsymbol{B}$ are given by (80).

Now we can conduct a surface stability analysis similar to the previous one, by using the moduli of (53). For the details see Ciarletta et al. (2013). Figure 13 displays the end result in the form of the $K^* - \Phi$ plots obtained for several values of the ratio β/μ. According to the Appendix, the quantity $8\beta/3\mu$ measures the infinitesimal matrix-to-fibres stiffness ratio. Here we consider in turn the cases $\beta/\mu = 0.0$ (no fibres), 0.8 (fibres softer than matrix), 2.0, and 4.0 (fibres stiffer than matrix.)

We remark that all the curves have a common point at $(K^*, \Phi) = (3.09, 73.3°)$, but this is an artefact due to the model. It can be explained by computing the components of the Stroh matrix in the coordinate system aligned with the Eulerian principal axes of deformation; see Ciarletta et al. (2013). Otherwise, the inclusion of fibres clearly makes the half-space more unstable in shear, as all the curves are below the isotropic $K^* = 3.09$ horizontal line. In the process of determining K^* numerically we also find that the wrinkle wavefronts are almost orthogonal to the fibres, in line with experimental observations, and also in line with the results of the previous subsection.
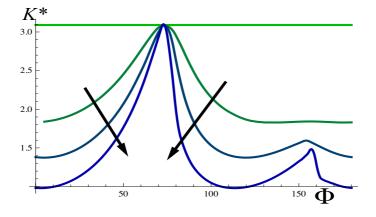
32

Figure 13. Bifurcation plots for surface instability of a neo-Hookean soft matrix with convex reinforcement in simple shear: Critical amount of shear K^* vs orientation Φ of the fibres in the reference configuration, for $\beta/\mu = 0.0, 0.8, 2.0, 4.0$ (increasing values indicated by arrows).

The main difference between the predictions of the standard reinforcing model (91) and of the anisotropic model of Ciarletta et al. (2011) is the disappearance of the discontinuities in the dispersion curves. This is to be expected, because of the strong convexity associated with the latter model. Whether one model is more accurate than the other (or accurate at all) is of course a matter for experimentalists to determine. This comment leads us naturally to the conclusion of this chapter, for which we invoke the wise recommendations of Golomb (1970).

5   Epilogue

The five DONT's of Modelling (Golomb, 1970)

1. Don't believe that the model is the reality;

2. Don't extrapolate beyond the region of fit;

3. Don't distort reality to fit the model;

4. Don't retain a discredited model;

5. Don't fall in love with your model.

A Appendix: Fibre to Matrix Stiffness Ratio

To compare the stiffness of the isotropic matrix to that of the fibres (in the case of a material reinforced with a single family of parallel fibres), we perform a tensile test in the direction of the fibres. For this test, the lateral contractions are equal by symmetry and the deformation gradient has components $\boldsymbol{F} = \mathrm{diag}\left(\lambda, \lambda^{-1/2}, \lambda^{-1/2}\right)$, where λ is the stretch ratio in the direction of uniaxial stretch. Then the left Cauchy–Green deformation tensor is $\boldsymbol{B} = \mathrm{diag}\left(\lambda^2, \lambda^{-1}, \lambda^{-1}\right)$, and $I_4 = \lambda^2$, $I_5 = \lambda^4$. It follows that the Cauchy stress has the following components

$$\sigma_1 = -p + 2W_1\lambda^2 - 2W_2\lambda^{-2} + 2W_4\lambda^2 + 4W_5\lambda^4,$$
$$\sigma_2 = \sigma_3 = 0 = -p + 2W_1\lambda^{-1} - 2W_2\lambda. \tag{115}$$

Subtracting one equation from the other to eliminate p, we find that

$$\sigma_1 = \lambda\widehat{W}'(\lambda), \quad \text{where} \quad \widehat{W}(\lambda) := W(\lambda^2 + 2\lambda^{-1}, \lambda^{-2} + 2\lambda, \lambda^2, \lambda^4). \tag{116}$$

When there is no stress ($\sigma_1 = 0$), there is no stretch ($\lambda = 1$), so that $\widehat{W}'(1) \equiv 0$. Then, for a small elongation, $\lambda = 1 + \epsilon$, say, we have by expansion of (116),

$$\sigma_1 = E_{11}\epsilon, \quad \text{where} \quad E_{11} = \widehat{W}''(1) \tag{117}$$

is the Young modulus in the fibre direction. Hence, in the case of the neo-Hookean standard reinforcing model (91), where

$$\widehat{W}(\lambda) = \mu(\lambda^2 + 2\lambda^{-1} - 3)/2 + E(\lambda^2 - 1)^2/4, \tag{118}$$

we find that

$$E_{11} = 3\mu + 2E, \tag{119}$$

In the case of the strain energy density (49), where

$$\widehat{W}(\lambda) = \mu(\lambda^2 + 2\lambda^{-1} - 3)/2 + \beta(\lambda - \lambda^{-1})^2, \tag{120}$$

we find that

$$E_{11} = 3\mu + 8\beta. \tag{121}$$

Bibliography

M. A. Biot. Surface instability of rubber in compression. *Applied Science Research, Series A*, 12:168–182, 1963.

Ph. Boulanger and M. Hayes. Finite-amplitude waves in deformed Mooney-Rivlin material. *Quarterly Journal of Mechanics and Applied Mathematics*, 45:575–593, 1992.

P. Chadwick. The application of the Stroh formalism to prestressed elastic media. *Mathematics and Mechanics of Solids*, 2:379–403, 1997.

P. Ciarletta, I. Izzo, S. Micera, and F. Tendick. Stiffening by fibre reinforcement in soft materials: A hyperelastic theory at large strains and its application. *Journal of the Biomechanical Behavior of Biomedical Materials*, 4:1359–1368, 2011.

P. Ciarletta, M. Destrade, and A. L. Gower. Shear instability in skin tissue. *Quarterly Journal of Mechanics and Applied Mathematics*, 66:273–288, 2013.

M. Destrade, M. D. Gilchrist, D. A. Prikazchikov, and G. Saccomandi. Surface instability of sheared soft tissues. *Journal of Biomechanical Engineering*, 130:061007, 2008.

J. N. Flavin. Surface waves in pre-stressed Mooney material. *Quarterly Journal of Mechanics and Applied Mathematics*, 16:441–449, 1963.

Y. B. Fu and A. Mielke. A new identity for the surface impedance matrix and its application to the determination of surface-wave speeds. *Proceedings of the Royal Society of London, Series A*, 458:2523–2543, 2002.

S. W. Golomb. Mathematical models–uses and limitations. *Simulation*, 4:197–198, 1970.

A. L. Gower and M. Destrade. Biot surface instability: Theory vs observation. submitted.

P. A. Meere, K. F. Mulchrone, and M. Timmerman. Shear folding in low-grade metasedimentary rocks: Reverse shear along cleavage at a high angle to the maximum compressive stress. *Geology*, 41:879–882, 2013.

J. Merodio and R. W. Ogden. Material instabilities in fiber-reinforced non-linearly elastic solids under plane deformation. *Archives of Mechanics*, 54:525–552, 2002.

A. Mielke and Y. B. Fu. Uniqueness of the surface-wave speed: A proof that is independent of the stroh formalism. *Mathematics and Mechanics of Solids*, 9:5–15, 2004.

M. J. P. Musgrave. *Crystal Acoustics*. Holden-Day, 1970.

R. W. Ogden. *Non-linear Elastic Deformations*. Dover, 1997.

R. W. Ogden. Elements of the theory of finite elasticity. In Y. B. Fu and R. W. Ogden, editors, *Nonlinear Elasticity: Theory and Applications*, pages 1–58. Cambridge University Press, 2001.

R. W. Ogden. Incremental statics and dynamics of pre-stressed elastic materials. In M. Destrade and G. Saccomandi, editors, *Waves in Nonlinear Pre-Stressed Materials, CISM Lecture Notes*, volume 495, pages 1–26. Springer, 2007.

N. H. Scott and M. Hayes. A note on wave propagation in internally constrained hyperelastic materials. *Wave Motion*, 7:601–605, 1985.

A. L. Shuvalov. On the theory of wave propagation in anisotropic plates. *Proceeding of the Royal Society of London, Series A*, 456:2197–2222, 2000.

C. Stolz. *Milieux Continus en Transformations Finies*. Editions de l'Ecole Polytechnique, 2010.

A. N. Stroh. Some analytic solutions for Rayleigh waves in cubic crystals. *Journal of Mathematics and Physics*, 41:77–103, 1962.

Q. Wang, Y. Yin, H. Xie, J. Liu, W. Yang, P. Chen, and Q. Zhang. Buckling modes of polymer membranes restricted by metal wires. *Soft Matter*, 7: 2888–2894, 2011.

J. P. Wolfe. Acoustic wavefronts in crystalline solids. *Physics Today*, September:34–40, 1995.